Ecological Indicators 145 (2022) 109609

Contents lists available at ScienceDirect

Ecological Indicators

journal homepage: www.elsevier.com/locate/ecolind

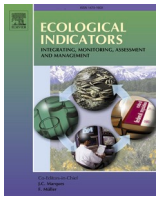

Variations in hydrological variables using distributed hydrological model in permafrost environment

Naveed Ahmed [a,b,*], Genxu Wang [c,*], Martijn J. Booij [d], Hero Marhaento [e], Foyez Ahmed Pordhan [f], Shahid Ali [h], Sarfraz Munir [i], Muhammad Zia-ur-Rehman Hashmi [g]

[a] Key Laboratory of Mountain Surface Process and Ecological Regulations, Institute of Mountain Hazards and Environment, Chinese Academy of Sciences, Chengdu 610041, China
[b] University of Chinese Academy of Sciences, Beijing 100049, China
[c] State Key Laboratory of Hydraulics and Mountain River Engineering, College of Water Resource and Hydropower, Sichuan University, Chengdu 610065, China
[d] Water Engineering and Management Group, Faculty of Engineering Technology, University of Twente, 7522 Enschede, the Netherlands
[e] Faculty of Forestry, Universitas Gadjah Mada, Yogyakarta 55281, Indonesia
[f] Department of Agricultural Extension and Rural Development, Bangabandhu Sheikh Mujibur Rahman Agricultural University, Gazipur 1706, Bangladesh
[g] Department of Civil Engineering, National University of Computer and Emerging Sciences, Foundation for Advancement of Science and Technology, Lahore 54000, Pakistan
[h] School of Science and Engineering, University of Kurdistan Hewler, 30 Meter Avenue, Erbil, Kurdistan 44001, Iraq
[i] Water Resources and Glaciology Section, Global Change Impact Studies Centre (GCISC), 6th Floor Emigration Tower, G-8/1, Islamabad 44000, Pakistan

ARTICLE INFO

Keywords:
Permafrost hydrology
SWAT model
Qinghai Tibet
Third Polar Region
Yangtze River
China

ABSTRACT

The Yangtze River Source Region (YaRSR) is located in the third polar region, the most threatened zone by global warming after the Arctic. Permafrost covers eighty percent of the total area of YaRSR, while the rest is seasonally frozen ground. Due to a significant rise in air temperature, degradation of the permafrost could occur. Permafrost coverage in a river basin greatly controls its hydrology. This study focuses on hydrological modeling in this permafrost environment using the Soil and Water Assessment Tool (SWAT). The SWAT model was calibrated (1985–2000) and validated (2001–2015) on a daily time step. The results were also compared on a monthly time scale. An impermeable layer was introduced within the SWAT model to represent the permafrost conditions. The streamflow is strongly dependent on the seasonal variation of precipitation and temperature, and the rising limb of the hydrograph shows the melting of snow, the contribution of soil water, and thawing of permafrost during the spring-summer season. The permafrost layer well restricted the deep percolation of water. During the spring season, streamflow mainly consists of surface runoff because of the frozen soils. Permafrost and frozen ground thawing lead to an increase in the contribution of groundwater flow to streamflow. Ultimately, the frozen ground depletes as the temperature gets close to the freezing point. This study also describes the SWAT model application to better analyze and understand the hydrology of the permafrost/frozen ground with limited data availability.

1. Introduction

Permafrost catchments in the Arctic and the Qinghai Tibetan Plateau (QTP) have been widely studied in recent decades. Numerous research works have been conducted in this direction, highlighting the changes in hydrological processes due to changes in climate and landcover/ use (e.g., human interventions and urbanization) (Bring et al., 2017; Fabre et al., 2017; Hülsmann et al., 2015; Song et al., 2020; Walvoord and Kurylyk, 2016). The QTP region is more significantly influenced by global climate change, outside the arctic pole (Serreze and Barry, 2011;

* Corresponding authors at: Key Laboratory of Mountain Surface Process and Ecological Regulations, Institute of Mountain Hazards and Environment, Chinese Academy of Sciences, Chengdu 610041, China (Naveed Ahmed); State Key Laboratory of Hydraulics and Mountain River Engineering, College of Water Resource and Hydropower, Sichuan University, Chengdu 610065, China (Genxu Wang).
E-mail addresses: naveedahmed@imde.ac.cn (N. Ahmed), wanggx@scu.edu.cn (G. Wang), m.j.booij@utwente.nl (M.J. Booij), marhaento@ugm.ac.id (H. Marhaento), foyez@bsmrau.edu.bd (F.A. Pordhan), shahid.ali@nu.edu.pk (S. Ali), s.munir@ukh.edu.krd (S. Munir), mhas074@aucklanduni.ac.nz (M.Z.-u.-R. Hashmi).

https://doi.org/10.1016/j.ecolind.2022.109609
Received 14 February 2022; Received in revised form 28 June 2022; Accepted 26 October 2022
Available online 31 October 2022

Zhao and Wu, 2019). Permafrost hydrology has not been investigated as much as the hydrology of catchments in lower to middle latitudes (Briggs et al., 2017; Woo et al., 2008). Detailed field investigations are required to understand the interaction between permafrost and hydrology. Data scarcity due to extreme weather conditions is one of the main obstacles to increase this understanding in arctic and sub-arctic regions (Romanovsky et al., 2010).

The research on permafrost hydrology was introduced in the early 1980 s and differed from hydrology in non-permafrost regions (Woo, 2012a, 2012b). Permafrost can affect interactions between surface and sub-surface water, soil–water heat exchange, and various hydrological processes in arctic and sub-arctic regions (Frampton and Destouni, 2015; Schramm et al., 2007; Walvoord et al., 2012). Permafrost accelerates surface runoff generation and shortens the runoff response to precipitation (McNamara et al., 1998; Woo, 2012b). The thermal soil regime, water storage dynamics, and evapotranspiration are also influenced by the presence of permafrost (Boike et al., 1998; Bowling et al., 2003; Hinzman et al., 2006; Hinzman et al., 1996). The active layer thickness plays a vital role in altering hydrological processes in permafrost regions (Woo, 2012a).

The Qinghai Tibetan Plateau (QTP) is also known as the Third Polar Region (TPR) due to its extreme climatic conditions. The runoff of river basins originating from QTP decreases in recent decades, and more than 1.4 billion people are dependent on these rivers (Immerzeel et al., 2010; Mao et al., 2016). Several studies were conducted to assess permafrost coverage and active layer thickness variations in the QTP (Zhao and Wu, 2019). Only a few modeling studies were done in this region due to the unavailability of long-term data. However, borehole data for very short time periods are available at some points, providing minimal soil freeze–thaw information (Cheng and Wu, 2007; Jin et al., 2007; Wu et al., 2010). Most of the models used to study permafrost distribution are conceptual and empirical models (e.g., temperature at the top of permafrost (TTOP) model, Stefan model, and Kudryavtsev model) (Kudryavtsev et al., 1974; Kudryavtsev et al., 1977; Smith and Riseborough, 1996). They are coupled with General Circulation Models (GCM) to predict future permafrost distribution and the threatened areas (Jiang et al., 2012; Qin et al., 2017; Zhang et al., 2013; Zhang and Wu, 2012). Zhou et al. (2013) investigated tundra and snowpack impacts on the active layer thickness using the Cold Regions Hydrological Model (CRHM) in western China. They found that there is delay in depletion of active layer thickness in the presence of soil organic matter and play barrier role under climate warming conditions. The main objective of this research was to understand the hydrological processes in a permafrost-affected catchment and to evaluate the influence of permafrost on the movement of surface runoff, lateral flow, and groundwater using distributed hydrological modeling approach, keeping in view the least data constraints and more flexibility. Moreover, there is neither any sensor installed for measuring the soil temperatures at various depths, nor the dynamic variations in active layer thickness recorded in the study area under-consideration in this article. Therefore, this is first step-forward to carry-out the understandings of the hydrological regime changes in the permafrost environment with data scarce regions.

2. Selection of hydrological model

Various models were applied to understand hydrological processes in cold regions (Bui et al., 2020). The Topoflow model is a process-based spatially distributed model used by (Schramm et al., 2007) and can simulate hydrological processes in permafrost regions. Topoflow model can simulate variations in Active Layer Thickness (ALT), snowmelt, the surface energy balance and infiltration (Bui et al., 2020). However, this model is not user-friendly and cannot be used for large catchments partially covered by continuous permafrost (Bui et al., 2020; Schramm et al., 2007). Moreover, the Topoflow model does not consider soil thermal properties at various depths (Fabre et al., 2017).

HBV is a conceptual semi-distributed hydrological model that was firstly applied in 1972 (Bergström, 1976; 1991). The HBV model has been numerously applied to estimate floods, climate change impacts on water resources, inflows to reservoirs and dams, etc. It can also deal with snowmelt, the surface energy balance, infiltration, and soil moisture (Bøggild et al., 1999; Osuch et al., 2019; Wawrzyniak et al., 2017). The HBV is also able to simulate the ALT (Bruland and Killingtveit, 2002). Nevertheless, the HBV shows limits in its calibration (Bergstrom, 2006). The model deals with the Thiessen polygon method to distribute daily temperature and precipitation, which give poor results (Bui et al., 2020).

The Cold Regions Hydrological Model (CRHM) is a modular-based physically-based, flexible hydrological model to simulate hydrological processes in small to medium cold watersheds from lumped to semi-distributed scales (Pomeroy et al., 2007). The model was applied in arctic to sub-arctic regions (Fang et al., 2013; Fang et al., 2010; Just, 2020; Pomeroy et al., 2012; Zhou et al., 2013). The CRHM uses Stefan's heat equation to simulate the ALT dynamics (Krogh et al., 2017). The CRHM simulates snow coverage excellently (Zhou et al. 2013). However, there is no calibration procedure to qualify the simulations, which makes it unreliable with high uncertainty (Bui et al., 2020).

The GEOtop model is also a physically-based, semi-distributed model with a coupled water and energy balance (Rigon et al., 2006). It is suitable to simulate surface temperature, glacier mass balances, thaw depth, groundwater table, soil water contents, and evapotranspiration (Bertoldi et al., 2006; Endrizzi and Marsh, 2010; Endrizzi et al., 2011; Gebremichael et al., 2009). The GEOtop model requires detailed input data (e.g., model parameters, field surveys, and experiments) and complex computation.

The WaSiM (water balance simulation model) is a fully distributed hydrological model developed by (Schulla, 1997). This model can be used on small to larger catchments ($>10^5$ km^2) from hourly to daily time steps. The WaSiM model can simulate the dynamics of the ALT, soil heat, and thawing depth. The WaSiM Model is highly sensitive to spatial and temporal resolutions. Due to its fully spatially distributed features, it needs a lot of input data and model parameters at a grid scale (Schulla and Jasper, 2007). In addition, it is not easy-to-use, especially for larger catchments having scarce input data.

The Soil and Water Assessment Tool (SWAT) is a physically-based semi-distributed hydrological model (Arnold et al., 1998). The SWAT model has been used in a vast range of areas from cold regions to tropical/ sub-tropical river basins (Ahmed et al., 2022b; Chiphang et al., 2020; Du et al., 2020; Duan et al., 2018; Marhaento et al., 2018; Nasab and Chu, 2020). The SWAT model can simulate from a sub-daily time step to an annual scale (Ahmed et al., 2022a; Arnold and Fohrer, 2005; Nasab and Chu, 2020). Moreover, complex hydrological systems can be modeled using SWAT (Fabre et al., 2017; Hülsmann et al., 2015; Melaku et al., 2020). The SWAT model can easily deal with watersheds of thousands of square kilometers (Nie et al., 2020). The SWAT model can simulate permafrost hydrology, snowmelt, surface energy balance, soil moisture, lateral flows, groundwater flow, and surface runoff in permafrost-covered areas (Fabre et al., 2017; Hülsmann et al., 2015). Moreover, the ALT can be modeled within the SWAT model but only using averaged values (Fabre et al., 2017; Hu et al., 2021; Hülsmann et al., 2015). The Fabre et al. (2017) simulated permafrost conditions using the SWAT model in a large Arctic watershed (2.54×10^6 km^2). Hülsmann et al. (2015) also successfully applied the SWAT model in the sub-arctic permafrost region of the Khara River basin in Northern Mongolia. This study focuses on a catchment of 140,000 km^2, situated in the Yangtze River Source Region (YaRSR) and uses the SWAT model. The SWAT model has proven its capability to simulate the permafrost conditions in cold regions in recent years (Fabre et al., 2017; Hülsmann et al., 2015), especially in data scarce regions with certain assumptions. This article also emphasize to explore the undersurface variations in the hydrological regimes in YaRSR to strengthen the understandings of hydrological processes in permafrost underlying areas of YaRSR.

3. Material and methods

3.1. Study area

The Yangtze River Source Region (YaRSR) is situated (90° 43′–96° 45′ E, 32° 30′–35° 35′ N) in the center of the Third Polar Region (TPR), located in the southwestern part of Qinghai Province (Fig. 1). The total drainage area of YaRSR at the Zhimenda hydrological gauging station is 140,000 km^2. There are 753 glaciers located in the YaRSR, which contribute to the streamflow (Guo et al., 2015). They deliver around 20 % of the total volume of water of the whole Yangtze River basin. The main channel originates from the glaciated areas of Tanggula mountain range (Fig. 1). Temperature has increased in the area since 1989 (Ahmed et al. (2020a), which might have consequences for the hydrology of the region. Precipitation in the YaRSR has also increased with a rate of 1.3 mm/year (Ahmed et al., 2020b) during 1961–2015.

The dominant land cover types in the watershed are grasslands, bare land, natural forests, glaciers, wetlands, natural lakes, and glaciers (Dong et al., 2002; Fujita and Ageta, 2000; Wang and Cheng, 2001; Wang et al., 2007; Yang et al., 2002), see Fig. 2. The Fig. 2 also shows the soil map, where most of the soils are Gleysols, Arenosols, Leptosols, and Cambisols. According to Zhao and Wu (2019), 80 % of the total area of the YaRSR is covered by permafrost, whereas the seasonally frozen ground covers about 20 % of the area (Fig. 2).

3.2. Data sources

The Digital Elevation Model (DEM) was obtained from the China Archive (https://www.igsnrr.ac.cn) with a scale of 1:250,000. The land cover/ land use raster files for the year 2015 were obtained from the Data Center for Resources and Environmental Sciences, Chinese Academy of Sciences (https://www.igsnrr.ac.cn) with a scale of 1:100,000. Raster files for soil data (1:1,000,000) were collected from the Harmonized World Soil Database V 1.2 (HWSD; FAO et al., 2009), which is a 30 arc-second database (http://webarchive.iiasa.ac.at/Research/LUC/External-World-soil-database). The daily streamflow data of one hydrological gauging station (Zhimenda station) from 1982 to 2015 was acquired from the Yangtze River Authority. The daily climatological variables (precipitation, maximum temperature, minimum temperature, mean temperature, wind speed, solar radiation, and relative humidity) from 1982 to 2015 were collected from the China Meteorological Administration (http://data.cma.cn). The latest permafrost distribution map was extracted from Zhao and Wu (2019).

3.3. Permafrost approach using soil and water Assessment Tool

The Soil and Water Assessment Tool (SWAT) version 2012 with ArcGIS 10.5 was used in this study. The elevation map, soil map and landcover map were used to create Hydrologic Response Units (HRUs). The HRUs are homogeneous units having similar soil, slope, and landcover properties (Arnold et al., 1998). Therefore, the whole area was divided into 8 sub-basins with 1737 HRUs. The daily climatic data from 1982 to 2015 was used to develop the SWAT model. The permafrost conditions were incorporated in the SWAT model using the approach developed by Hülsmann et al. (2015) for Northern Mongolia. The impervious layer was implemented in the SWAT model to depict the

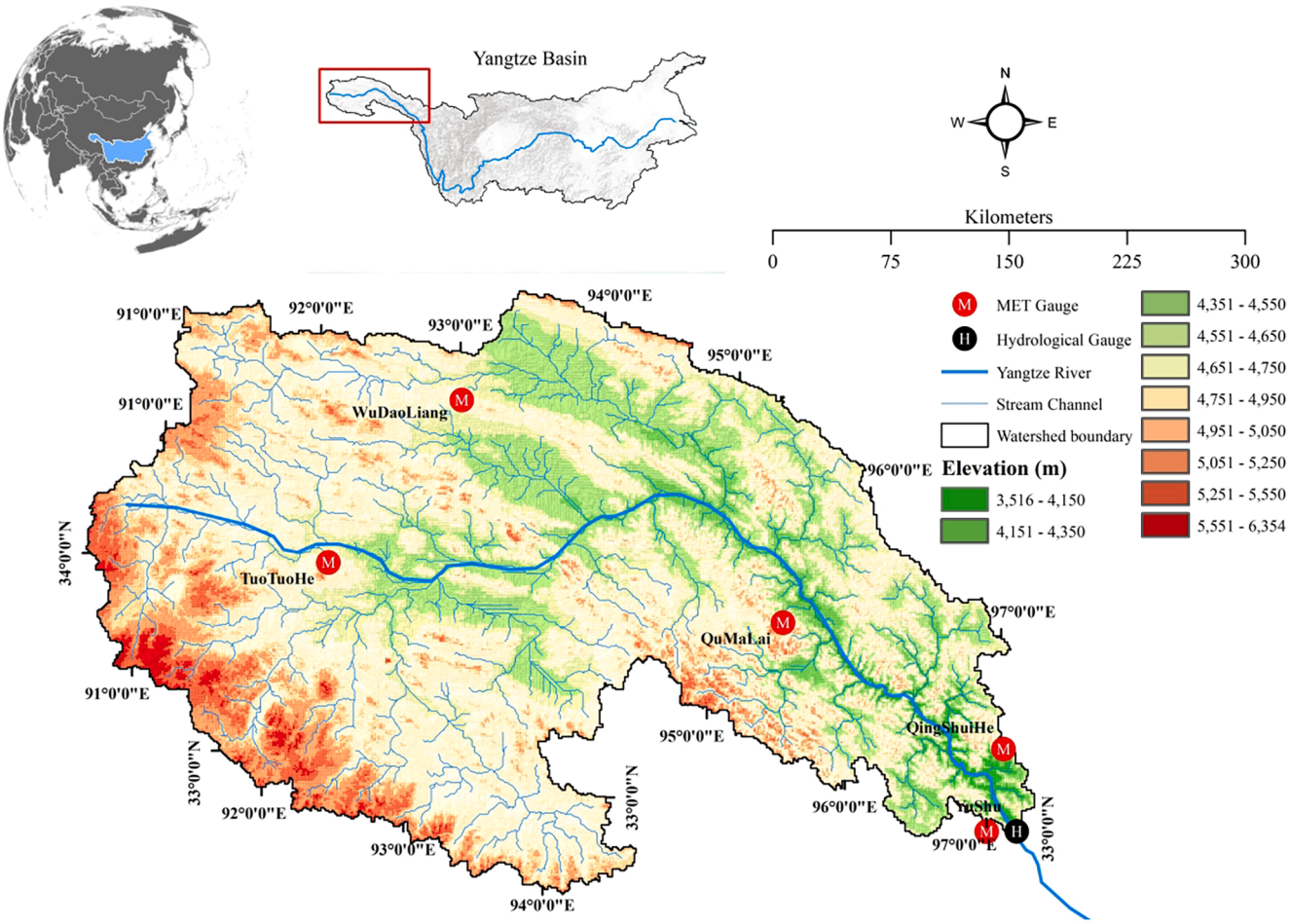

Fig. 1. The Yangtze River Source Region (YaRSR) with hydrological and meteorological stations.

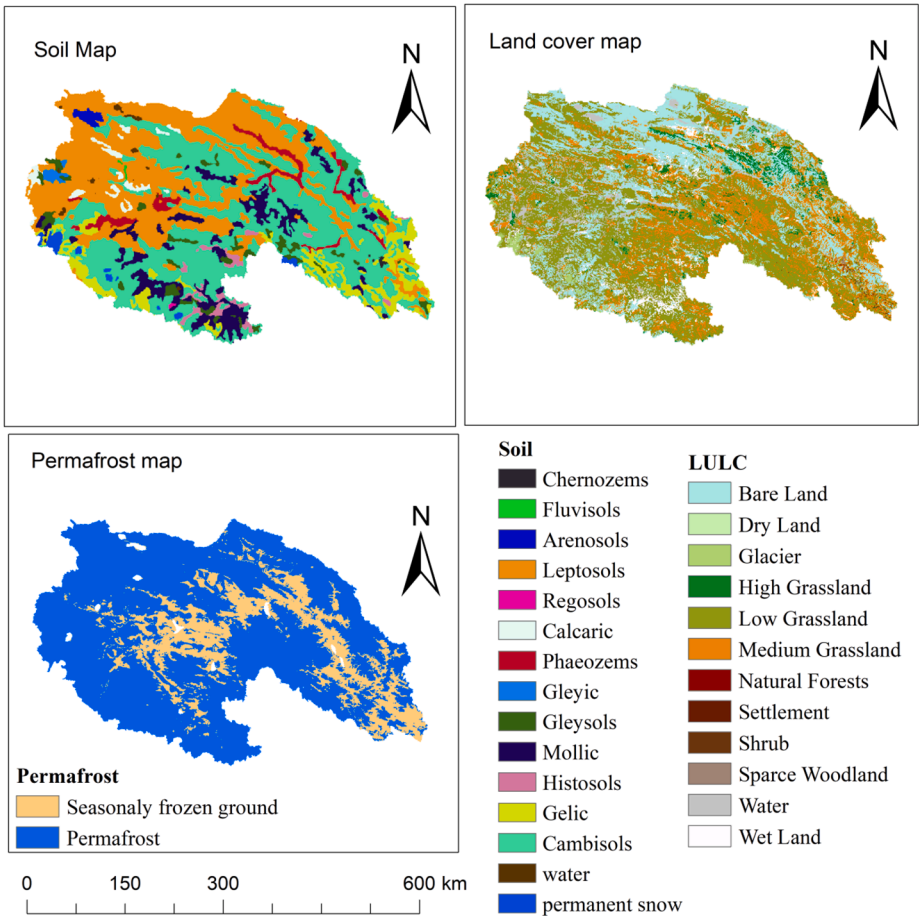

Fig. 2. The soil, land cover and permafrost distribution in the Yangtze River Source Region.

bottom of the ALT within the permafrost soils. This layer prevents deep percolation of water from the active layer and surface soils (Woo, 2012a). Ultimately, permafrost acts as a barrier to prevent recharge of groundwater and hence restricts groundwater flow and discharge to unfrozen areas. Therefore, the bottom of the ALT was obtained from Zhao and Wu (2019) and provided in the SWAT model to simulate the behavior of permafrost as a barrier for groundwater recharge. An averaged depth of 2.1 m was provided in the SWAT model. However, this model setting neglects the temporal development and gradual thawing and freezing of the active layer.

4. Model calibration and validation

The SWAT model was simulated for daily discharge from January 1985 to December 2015. The calibration period was selected from 1985 to 2000, and the validation period from 2001 to 2015. The period from 1982 to 1984 was selected as the model spin-up/warm-up period. The Sequential Uncertainty Fitting version 2 (SUFI-2) provided in SWAT-CUP version 2019 was used for calibration (Abbaspour et al., 2004; Abbaspour et al., 2015). The calibration with the SUFI-2 algorithm in SWAT-CUP was done in 5 iterations within each iteration 500 simulations to achieve the best fitted sensitive parameters. The simulated daily streamflow was compared with the observed streamflow. The Kling Gupta Efficiency (KGE) was selected as objective function to evaluate the model in the calibration and validation (Gupta et al., 2009; Magnusson et al., 2015; Nicolle et al., 2014)..

Four criteria were selected to compare observed and simulated streamflow in the calibration and validation: the Kling Gupta Efficiency, the Nash-Sutcliffe Efficiency (NSE), the coefficient of determination (R^2), and the Percentage of Bias (PBIAS). A detailed description of these evaluation criteria is provided below:

$$KGE = 1 - \sqrt{(R-1)^2 + (\beta-1)^2 + (\alpha-1)^2}$$

$$\beta = \frac{\mu_{sim}}{\mu_{obs}}$$

$$\alpha = \frac{\mathrm{CV_{sim}}}{\mathrm{CV_{obs}}} \quad (1)$$

$$NSE = 1 - \frac{\sum_{i=1}^{N}\left[Q_{obs,i} - Q_{sim,i}\right]^2}{\sum_{i=1}^{N}\left[Q_{obs,i} - Q_{\overline{obs}}\right]^2} \quad (2)$$

$$R^2 = \frac{\left[\sum_{i=1}^{N}\left(Q_{obs,i} - Q_{mean,i}\right)\left(Q_{sim,i} - Q_{mean,i}\right)\right]^2}{\sum_{i=1}^{N}\left(Q_{obs,i} - Q_{mean,i}\right)^2 \sum_{i=1}^{N}\left(Q_{sim,i} - Q_{mean,i}\right)} \quad (3)$$

$$PBIAS = \frac{\sum_{i=1}^{N}\left(Q_{sim,i} - Q_{obs,i}\right)}{\sum_{i=1}^{N} Q_{obs,i}} \times 100 \quad (4)$$

Where$Q_{obs,i}$,$Q_{mean,i}$, and $Q_{sim,i}$ are observed, mean observed, and simulated flows, respectively. The NSE ranges between -∞ and 1 and defines the fit between observed and simulated values with an optimal value of 1 (Nash and Sutcliffe, 1970). Negative and positive values for the percentage bias (PBIAS) represent underestimation and overestimation of the model, whereas a value of zero is the ideal condition (Moriasi et al., 2007). KGE incorporates the correlation coefficient (R), the bias and the similarity of observed and simulated standard deviation. Symbol μ is the average, CV the coefficient of variation, β is the bias and α is the ratio of simulated and observed standard variation (Dick et al.,

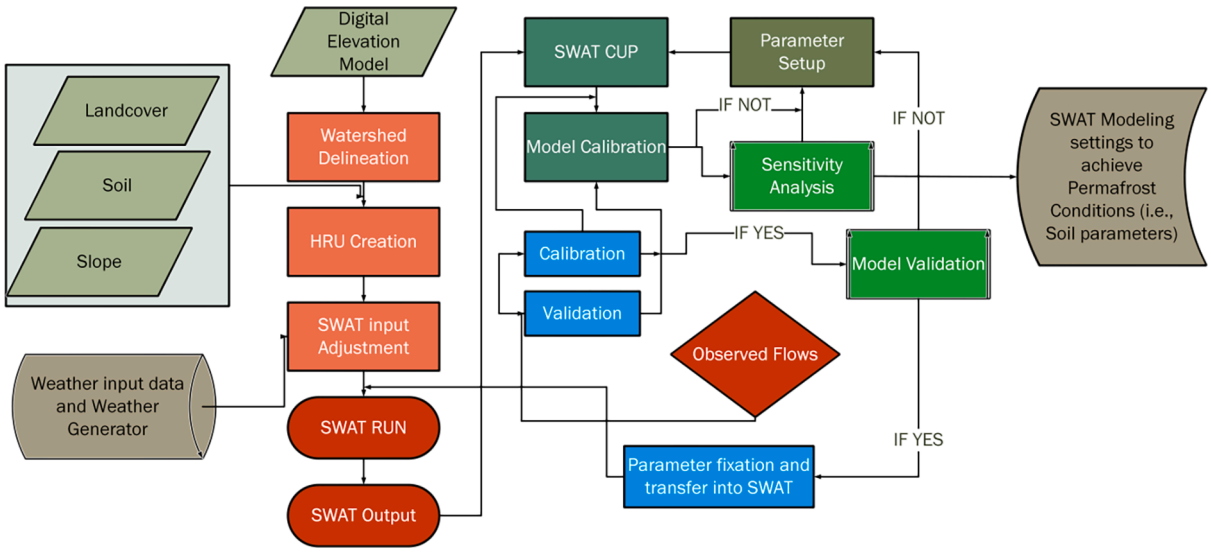

Fig. 3. Flowchart of SWAT Model with permafrost settings.

2015). A KGE value equal to 1 shows that simulated flows are identical to observed flows. The flowchart of SWAT model with permafrost settings is illustrated in Fig. 3.

5. Results and discussion

5.1. Simulated daily streamflow regimes

The list of best-fit sensitive parameters along with optimal values can be found in Annexure-I. The objective function KGE was 0.81 for daily simulation in the calibration period (1985–2000) in Fig. 4 and 0.71 in the validation period (2001–2015) as shown in Fig. 5. The YaRSR streamflow is dominated by peak flows in the summer season due to snow melting in May and June and heavy precipitation in July and August. In winter, the streamflow is mainly determined by the decrease of base flow. The calibrated model strongly underestimated streamflow in 1990 (PBIAS = 19.71), while it overestimated streamflow in 1997 (PBIAS = -59.96). The highest value of KGE (0.89) was found in 1989, where the model was underestimating medium flows (~1500–2000 m^3/s (Fig. 4). During the validation period (2001–2015), the overall model performance was good (KGE = 0.71 and PBIAS = -1.39). The model overestimated streamflow in 2002, 2008, and 2010–2014. The highest value of KGE (0.88) was found in 2007. The NSE and R^2 values for the calibration and validation period are also in an acceptable range as defined by Moriasi et al. (2007). The statistics of the evaluation criteria for the entire calibration and validation periods are presented in Figs. 4

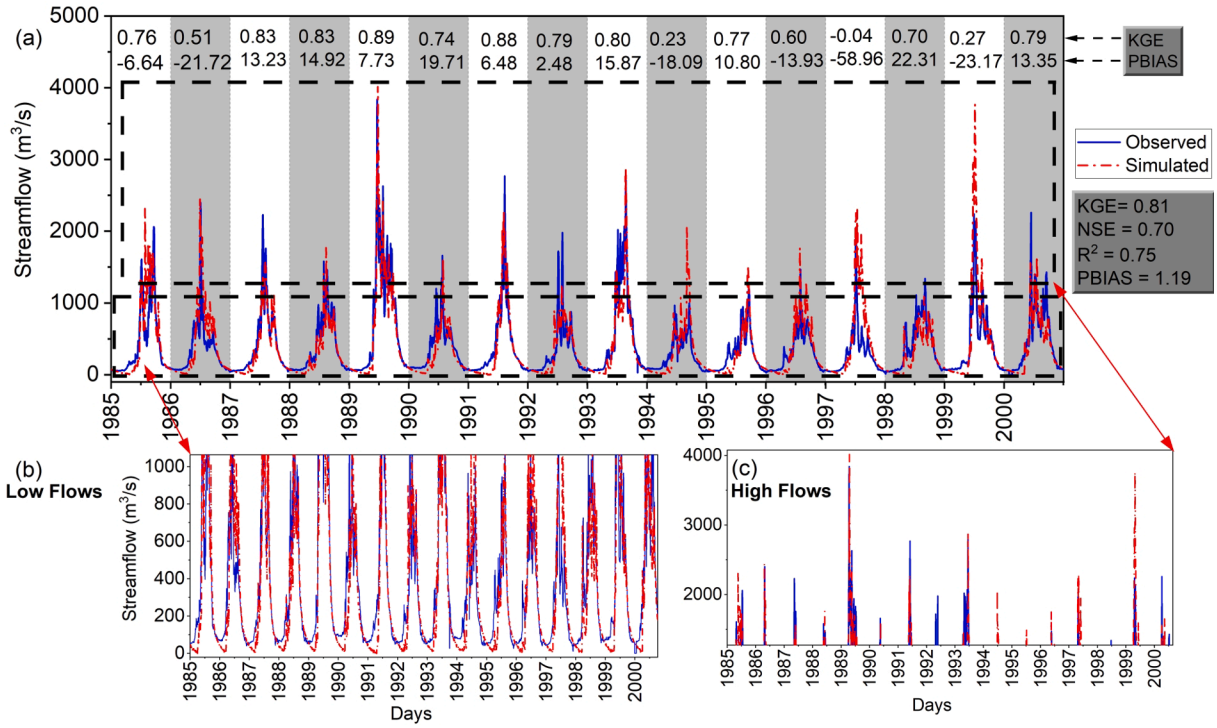

Fig. 4. Daily observed and simulated streamflow at Zhimenda hydrological station during the calibration period (1985–2000) in figure (a), Low flows and high flows are also given in sub-figure (b) and (c).

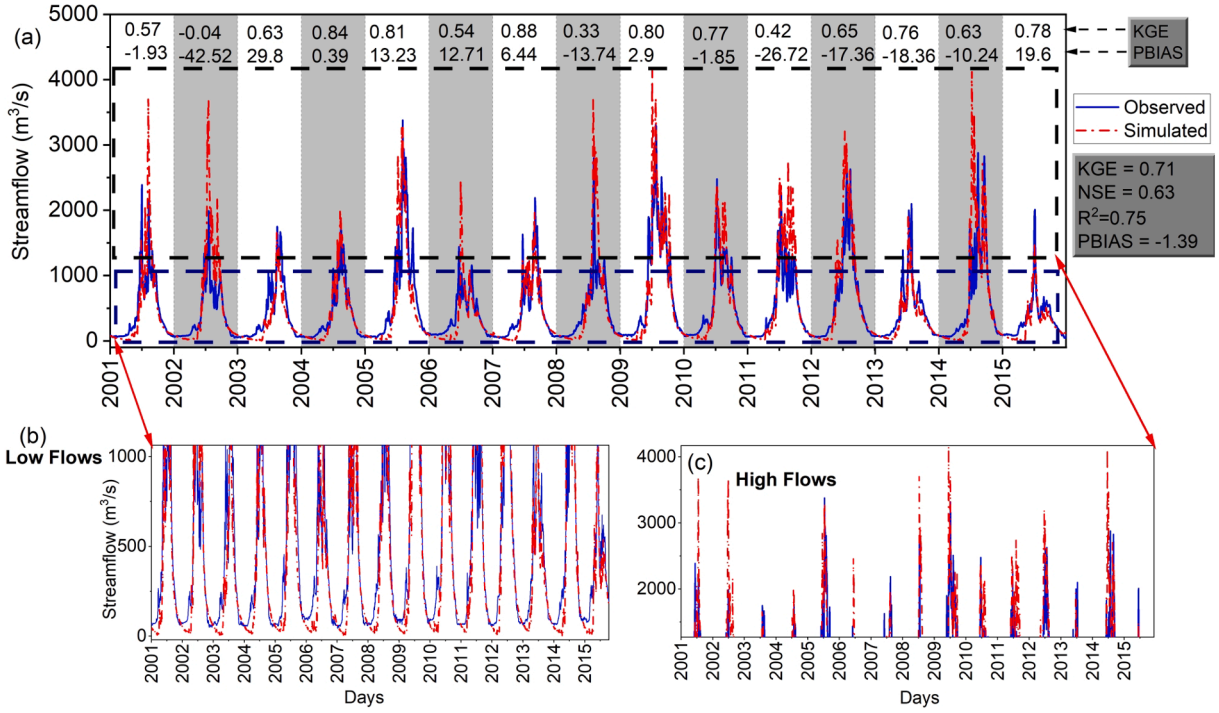

Fig. 5. Daily observed and simulated streamflow at Zhimenda hydrological station during the validation period (2001–2015) in figure (a), Low flows and high flows are also given in sub-figure (b) and (c).

and 5 as well. The daily low flows are well captured by sensitive parameters selected by SWAT-CUP during calibration and validation period; however, the selected parameters over/under-estimated the high flows. The surface flow is also accelerated due to increase in precipitation as well as melting of the snow simultaneously. Moreover, the high flows contributed to surface runoff while low flows mainly accelerated the groundwater and lateral flows due to introducing of impermeable layer at 2.1 m depth.

5.2. Comparison between daily and monthly simulations

Figs. 6 and 7 compares monthly observed and simulated hydrographs with daily observed and simulated hydrographs in the calibration period (1985–2000). The objective function KGE for monthly

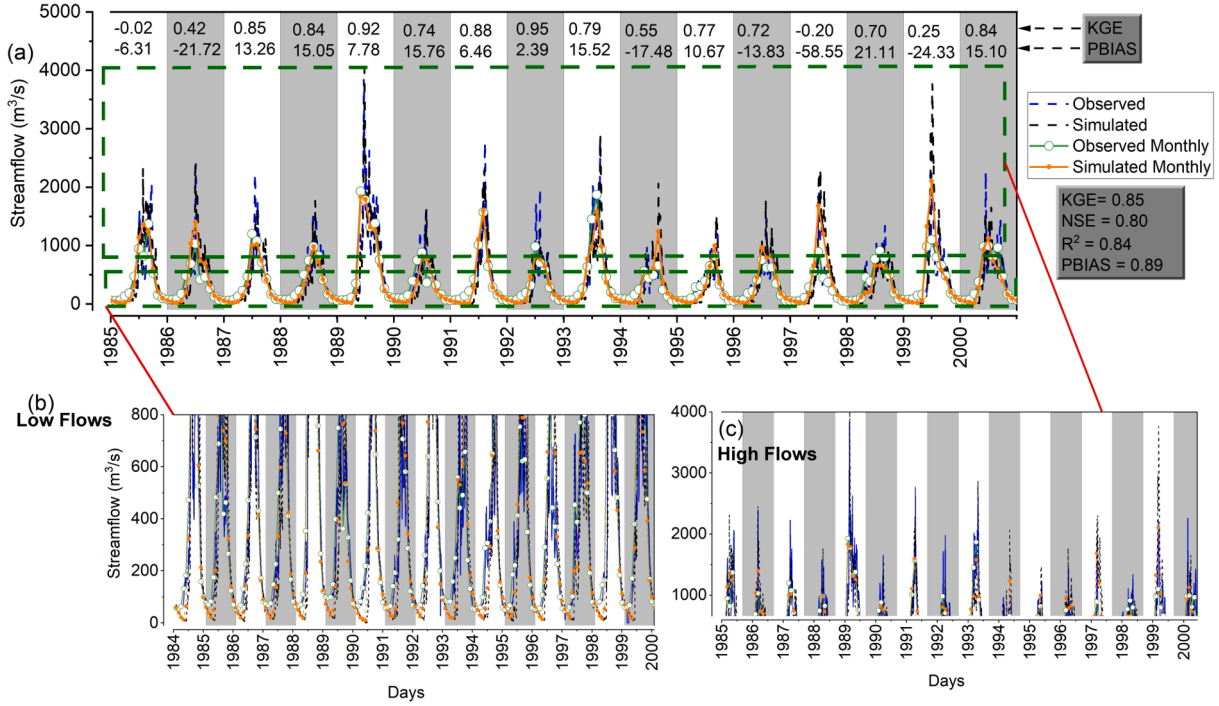

Fig. 6. Monthly observed and simulated streamflow at Zhimenda hydrological station during calibration period (1985–2000) in figure (a), low flows and high flows are also given in sub-figure (b) and (c).

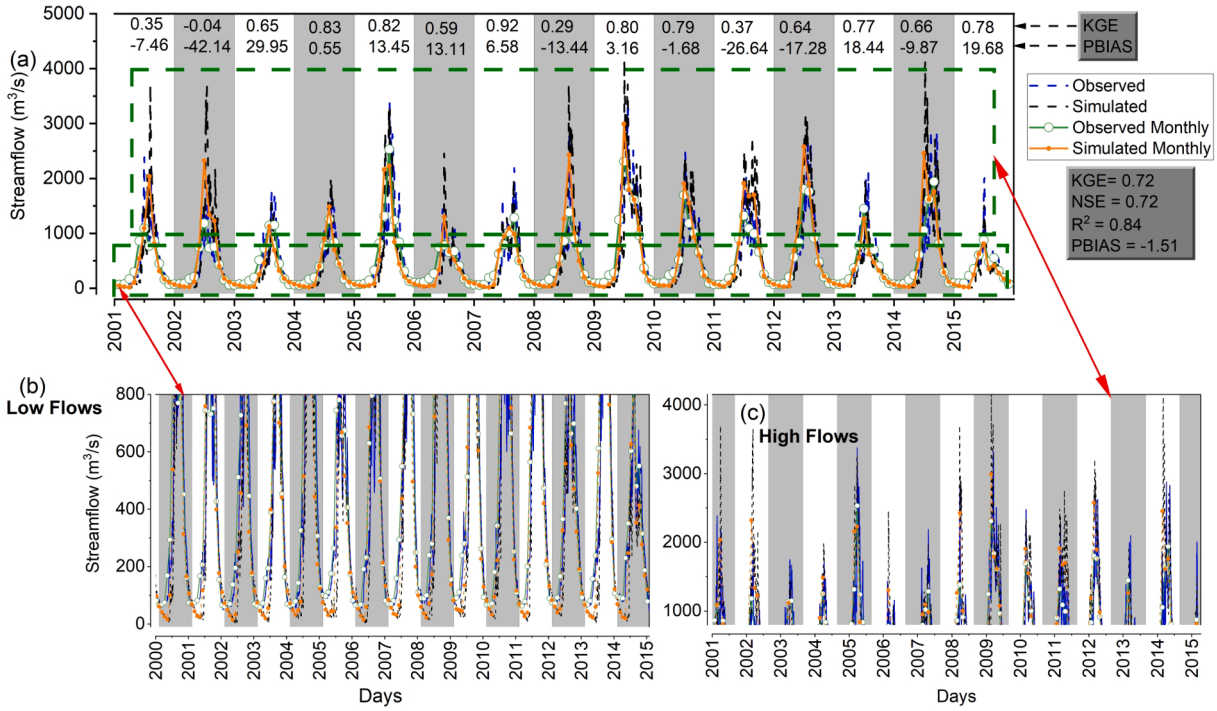

Fig. 7. Monthly observed and simulated streamflow at Zhimenda hydrological station during validation period (2001–2015) in figure (a), low flows and high flows are also given in sub-figure (b) and (c).

simulations is 0.85, and PBIAS is 0.89 (Fig. 6). It shows that there is a small difference between observed and simulated monthly streamflow. NSE and R^2 values are 0.80 and 0.84, respectively, for the entire calibration period (Fig. 6). The model well captured the low and peak flows throughout the calibration period, whereas some peaks were overestimated (PBIAS negative), especially in 1997, where PBIAS was −58.55. The highest KGE value (0.95) was found in 1992, followed by 0.92 in 1989. The annual values of KGE and PBIAS are also presented in Fig. 5 for the calibration and validation period. Similar to Figs. 4 and 5, the monthly flows simulations were well captured for low flows as compared to high flows.

Fig. 7 showed the validation period (2001–2015), the KGE value is 0.71, with a minor overestimation of the model (PBIAS = -1.51). The values of NSE and R^2 were also good, being 0.72 and 0.84, respectively. On annual basis, the highest overestimation was found in 2002 (PBIAS = -42.14), and the highest KGE value (0.92) was found in 2007 during

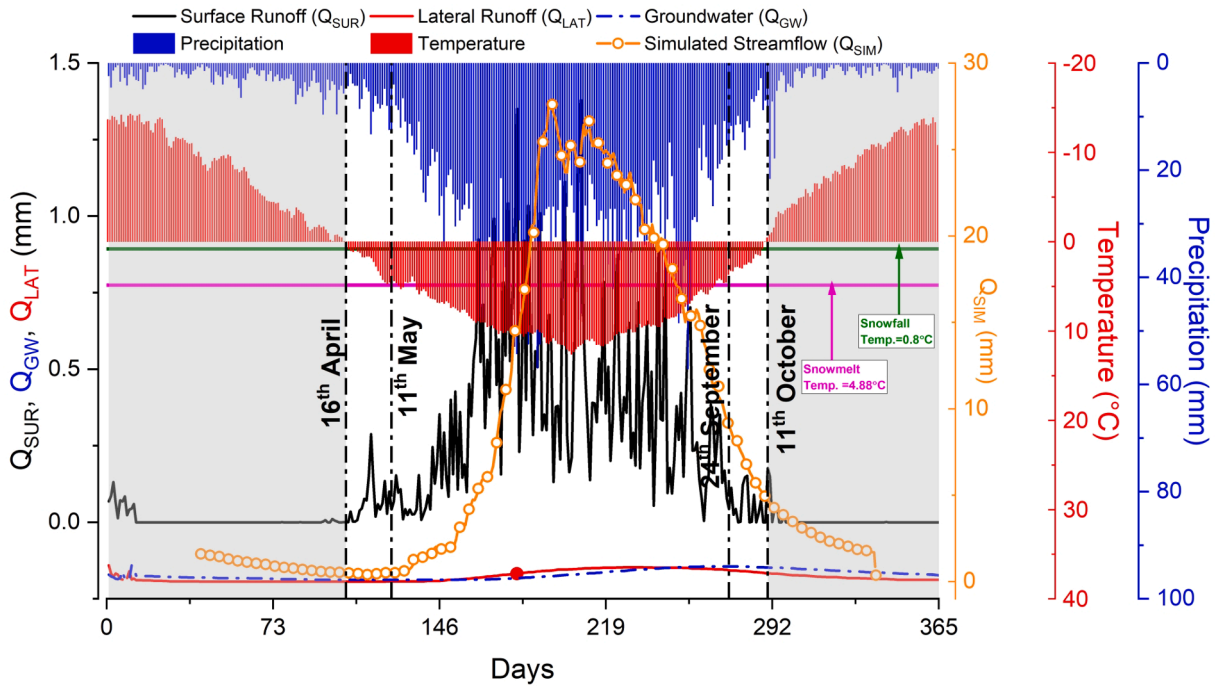

Fig. 8. The modeled daily water balance components including Surface Runoff (mm), Lateral flow (mm), and Groundwater flow (mm) for entire period (1985–2015) in YaRSR considering permafrost conditions.

the validation period. It can also be observed from Figs. 6 and 7 that the monthly simulations show overestimations and underestimations in the same years as the daily simulations, however, the values of PBIAS and KGE varied between daily and monthly simulations. This also shows the robustness of the SWAT model to well capture the hydrological modeling of cold regions.

5.3. Water balance under permafrost conditions

The SWAT model simulations from 1985 to 2015 were also carried out to estimate the water balance components under permafrost conditions. Fig. 8 shows the average daily (1985–2015) simulations of streamflow (Q_{SIM}), surface runoff (Q_{SUR}), groundwater flow (Q_{GW}), lateral flow (Q_{LAT}), average temperature, and precipitation for the entire YaRSR catchment. Fig. 5 is divided into five different parts based on the snowfall temperature (0.8℃) and the snowmelt temperature (4.88 ℃), two parameters of the SWAT model (see Appendix-I). The temperature is negative from the start of the year to 16th of April, leading to Q_{SUR}, Q_{GW} and Q_{LAT} values around zero. After this date, the temperature increases, resulting in the rise of Q_{SUR} while snowmelt starts to contribute to Q_{SUR} from 11th of May as the modeled snowmelt temperature is above 4.88 ℃. From May to September, snowmelt and precipitation contribute simultaneously to the streamflow. The Q_{SUR} is decreasing as the temperature starts to decrease (24th September) and becomes zero again on the 11th October. However, Q_{LAT} is higher in June and July due to permafrost thawing, while Q_{GW} is found higher in September and October. Q_{SUR} reaches its maximum contribution in the mid of July, while Q_{LAT} starts decreasing at the end of July. During this period, Q_{SUR} is still dominant as permafrost is not completely thawed. Though, Q_{LAT} and Q_{GW} are very limited due to the impervious layer (permafrost) settings in the SWAT model. After the 24th September, Q_{LAT} becomes zero due to the freezing of permafrost whereas there is very little amount of Q_{GW}. The latter also becomes zero as the soil freezes again. Meanwhile, Q_{SIM} is also decreasing. Fig. 8 also illustrates that the permafrost behavior is well modeled in SWAT. The temperature is a key component driving the variations of the hydrological components with snowmelt and snowfall in permafrost environments.

5.4. Discussion

The permafrost hydrological modeling approach conducted in this study resulted in a very good representation of the water components in the YaRSR region. The simulated hydrographs are close to observations on a daily time step as well as on a monthly scale (Figs. 4 – 7). The daily simulated hydrograph shows that the streamflow is strongly dependent on the seasonal variation of precipitation and temperature (Ahmed et al., 2020b). The increasing limb of the hydrograph shows the melting of snow, the contribution of soil water, and permafrost thawing during the spring-summer season (Hülsmann et al., 2015; Woo et al., 2000). The permafrost layer well restricted the deep percolation of water, as Hülsmann et al. (2015) stated for the Khara River basin in Mongolia as well. The results of this study are consistent with the findings of Fabre et al. (2017) for an Arctic watershed using a similar approach in SWAT model. Fabre et al. (2017) also introduced an impermeable layer in the arctic watershed which shows the permafrost bottom and achieve the permafrost phenomenon in SWAT model settings. The snowmelt water does not simultaneously contribute to streamflow in permafrost environments. However, it contributed to surface runoff (Woo, 2012a).

In SWAT, the soils are frozen, and there is no further penetration of frost into the ground, which ultimately results in the decrease of hydraulic conductivity of soils. Consequently, the permafrost layer acts as an impermeable layer to limit the lateral and groundwater movement (Williams, 1970; Woo and Winter, 1993). The permafrost representation in the SWAT model was obtained by introducing an impermeable layer (i.e., the bottom of the permafrost layer) at 2.1 m, a value defined based on Zhao and Wu (2019). The SWAT model does not deal with the soil-heat transfer mechanism. Therefore, it is not possible to simulate the temporal and spatial variations of the permafrost active layer thickness.

Moreover, SWAT has well proved to be applicable for an average permafrost layer to be modeled (Fabre et al., 2017; Hülsmann et al., 2015). It is also clear from this study that the distribution of permafrost controls the hydrology of a river basin and the surface–subsurface water movement (Walvoord et al., 2012; Woo et al., 2008). This study is a new way forward and contribution to permafrost hydrological modeling studies. In this study, we have shown the behavior of water balance components on a daily time scale in this region, and we have provided detailed information on hydrological features. However, the SWAT model results can be compared to any other suitable model with minimum input data requirement. Moreover, the SWAT model can be upgraded to simulate the dynamic freezing/thawing of active layer thickness.

6. Conclusion

This study aimed to model the variations in water balance components in a river basin with permafrost coverage. model. The permeable layer was introduced into the SWAT model settings at a depth of 2.1 m which limits the sub-surface water movement. The snowfall and snowmelt temperatures of 0.8 ℃ and 4.88 ℃ were obtained from model simulations, respectively.. The conclusions are summarized as:

- Surface Runoff (Q_{SUR}), Groundwater flow (Q_{GW}), and Lateral flow (Q_{LAT}) were zero until the snowmelt starts (11th of May).
- The snowmelt contributes to the hydrological components from May to September simultaneously with precipitation.
- The Q_{SUR} is dominant during the peak flow period.
- Simulated discharge and Q_{SUR} start to decrease as the temperature decreases (24th of September).
- Finally, Q_{SUR} becomes zero as the snow is stored on the land again (11th of October).

This was the first effort in the Yangtze River Source Region (YaRSR) in the Third Polar Region to simulate the permafrost hydrology using the SWAT The above findings also depicts that the temperature is a key component driving the variations in hydrological components due to snowmelt and snowfall in permafrost environments.

7. Limitations and uncertainties

The major contingency of the method used in this study is the assumption that in-tractions among various factors were neglected. However, climate change and land-cover change can change the regional hydrology. Additionally, the choice of hydrological models, length of the data sets available, and hydro-meteorological data quality may also affect the results (Ahmed et al., 2022b). The SWAT model used in this study deals with the surface water hydrological interactions whereas the dynamic variations (thawing/freezing) of permafrost active layer thickness is not possible (Bui et al., 2020; Hu et al., 2021; Melaku et al., 2020). Therefore, we introduced the fixed layer of permafrost and this is the limitation of this study. However, this is a first step forward to simulate the SWAT model in this study area in context of permafrost which indeed will be a way-forward to further modified the SWAT model as well as subsurface hydrology of this region.

CRediT authorship contribution statement

Naveed Ahmed: Conceptualization, Methodology, Software, Investigation, Writing – original draft, Funding acquisition, Formal analysis, Resources, Data curation, Project administration. **Genxu Wang:** Investigation, Visualization, Supervision, Writing – review & editing. **Martijn J. Booij:** Investigation, Visualization, Supervision, Writing – review & editing. **Hero Marhaento:** Investigation, Visualization, Supervision,

Writing – review & editing. **Foyez Ahmed Pordhan:** Formal analysis, Resources, Data curation, Project administration, Writing – review & editing. **Shahid Ali:** Formal analysis, Resources, Data curation, Project administration, Writing – review & editing. **Sarfraz Munir:** Software, Investigation, Visualization, Supervision, Writing – review & editing. **Muhammad Zia-ur-Rehman Hashmi:** Software, Investigation, Visualization, Supervision, Writing – review & editing.

Declaration of Competing Interest

The authors declare that they have no known competing financial interests or personal relationships that could have appeared to influence the work reported in this paper.

Acknowledgments

This work was financially supported by the National Natural Science Foundation of China (No. U2240226). The first author would also like to express his sincere thankfulness to the Chinese Academy of Sciences and The World Academy of Sciences (CAS-TWAS) for providing a fellowship for the doctoral degree (Awardee of 2017, CAS-TWAS President's Fellowship). The authors are very thankful to the China Meteorological Administration (CMA), the Yangtze River Authority, Food and Agriculture Organization (FAO), and Data Center for Resources and Environmental Sciences, Chinese Academy of Sciences, to share data used in this study.

Appendix A. Supplementary data

Supplementary data to this article can be found online at https://doi.org/10.1016/j.ecolind.2022.109609.

References

Abbaspour, K.C., Johnson, C., Van Genuchten, M.T., 2004. Estimating uncertain flow and transport parameters using a sequential uncertainty fitting procedure. Vadose Zone J. 3 (4), 1340–1352.
Abbaspour, K.C., Rouholahnejad, E., Vaghefi, S., Srinivasan, R., Yang, H., Kløve, B., 2015. A continental-scale hydrology and water quality model for Europe: Calibration and uncertainty of a high-resolution large-scale SWAT model. J. Hydrol. 524, 733–752.
Ahmed, N., Wang, G., Booij, M.J., Oluwafemi, A., Hashmi, M.Z.-u.-R., Ali, S. and Munir, S. 2020b. Climatic Variability and Periodicity for Upstream Sub-Basins of the Yangtze River, China. Water 12(3), 842.
Ahmed, N., Wang, G.-X., Oluwafemi, A., Munir, S., Hu, Z.-Y., Shakoor, A., Imran, M.A., 2020a. Temperature trends and elevation dependent warming during 1965–2014 in headwaters of Yangtze River, Qinghai Tibetan Plateau. J. Mountain Sci. 17 (3), 556–571.
Ahmed, N., Wang, G., Booij, M.J., Xiangyang, S., Hussain, F., Nabi, G., 2022a. Separation of the Impact of Landuse/Landcover Change and Climate Change on Runoff in the Upstream Area of the Yangtze River, China. Water Resour. Manage. 36 (1), 181–201.
Ahmed, N., Wang, G., Lü, H., Booij, M.J., Marhaento, H., Prodhan, F.A., Ali, S., Ali Imran, M., 2022b. Attribution of Changes in Streamflow to Climate Change and Land Cover Change in Yangtze River Source Region, China. Water 14 (2), 259.
Arnold, J.G., Fohrer, N., 2005. SWAT2000: current capabilities and research opportunities in applied watershed modelling. Hydrolog. Process.: Int. J. 19 (3), 563–572.
Arnold, J.G., Srinivasan, R., Muttiah, R.S., Williams, J.R., 1998. Large area hydrologic modeling and assessment part I: model development 1. JAWRA J. Am. Water Resour. Assoc. 34 (1), 73–89.
Bergström, S., 1991. Principles and Confidence in Hydrological Modelling. Hydrol. Res. 22 (2), 123–136.
Bergstrom, S., 2006. Experience from applications of the HBV hydrological model from the perspective of prediction in ungauged basins. IAHS Publ. 307, 97.
Bergström, S., 1976. Development and application of a conceptual runoff model for Scandinavian catchments.
Bertoldi, G., Rigon, R., Over, T.M., 2006. Impact of Watershed Geomorphic Characteristics on the Energy and Water Budgets. J. Hydrometeorol. 7 (3), 389–403.
Bøggild, C., Knudby, C., Knudsen, M., Starzer, W., 1999. Snowmelt and runoff modelling of an Arctic hydrological basin in west Greenland. Hydrol. Process. 13 (12–13), 1989–2002.
Boike, J., Roth, K., Overduin, P.P., 1998. Thermal and hydrologic dynamics of the active layer at a continuous permafrost site (Taymyr Peninsula, Siberia). Water Resour. Res. 34 (3), 355–363.
Bowling, L.C., Kane, D.L., Gieck, R.E., Hinzman, L.D., Lettenmaier, D.P., 2003. The role of surface storage in a low-gradient Arctic watershed. Water Resour. Res. 39 (4).
Briggs, M.A., Campbell, S., Nolan, J., Walvoord, M.A., Ntarlagiannis, D., Day-Lewis, F.D., Lane, J.W., 2017. Surface Geophysical Methods for Characterising Frozen Ground in Transitional Permafrost Landscapes. Permafrost Periglac. Process. 28 (1), 52–65.
Bring, A., Shiklomanov, A., Lammers, R.B., 2017. Pan-Arctic river discharge: Prioritizing monitoring of future climate change hot spots. Earth's Future 5 (1), 72–92.
Bruland, O., Killingtveit, Å., 2002. Application of the HBV-model in Arctic catchments–some results from Svalbard.
Bui, M.T., Lu, J., Nie, L., 2020. A Review of Hydrological Models Applied in the Permafrost-Dominated Arctic Region. Geosciences 10 (10), 401.
Cheng, G., Wu, T., 2007. Responses of permafrost to climate change and their environmental significance, Qinghai-Tibet Plateau. J. Geophys. Res. Earth Surf. 112 (F2).
Chiphang, N., Bandyopadhyay, A., Bhadra, A., 2020. Assessing the Effects of Snowmelt Dynamics on Streamflow and Water Balance Components in an Eastern Himalayan River Basin Using SWAT Model. Environ. Model. Assess. 25 (6), 861–883.
Dick, J.J., Tetzlaff, D., Birkel, C., Soulsby, C., 2015. Modelling landscape controls on dissolved organic carbon sources and fluxes to streams. Biogeochemistry 122 (2), 361–374.
Dong, S., Zhou, C., Wang, H., 2002. Ecological crisis and countermeasures of the Three Rivers Headstream Regions. J. Natural Resour. 17 (6), 713–720.
Du, X., Goss, G., Faramarzi, M., 2020. Impacts of Hydrological Processes on Stream Temperature in a Cold Region Watershed Based on the SWAT Equilibrium Temperature Model. Water 12 (4), 1112.
Duan, Y., Liu, T., Meng, F., Luo, M., Frankl, A., De Maeyer, P., Bao, A., Kurban, A., Feng, X., 2018. Inclusion of modified snow melting and flood processes in the swat model. Water 10 (12), 1715.
Endrizzi, S., Marsh, P., 2010. Observations and modeling of turbulent fluxes during melt at the shrub-tundra transition zone 1: point scale variations. Hydrol. Res. 41 (6), 471–491.
Endrizzi, S., Quinton, W.L., Marsh, P., 2011. Modelling the spatial pattern of ground thaw in a small basin in the arctic tundra. Cryosphere Discuss. 2011, 367–400.
Fabre, C., Sauvage, S., Tananaev, N., Srinivasan, R., Teisserenc, R., Sánchez Pérez, J.M., 2017. Using modeling tools to better understand permafrost hydrology. Water 9 (6), 418.
Fang, X., Pomeroy, J.W., Westbrook, C.J., Guo, X., Minke, A.G., Brown, T., 2010. Prediction of snowmelt derived streamflow in a wetland dominated prairie basin. Hydrol. Earth Syst. Sci. 14 (6), 991–1006.
Fang, X., Pomeroy, J.W., Ellis, C.R., MacDonald, M.K., DeBeer, C.M., Brown, T., 2013. Multi-variable evaluation of hydrological model predictions for a headwater basin in the Canadian Rocky Mountains. Hydrol. Earth Syst. Sci. 17 (4), 1635–1659.
Frampton, A., Destouni, G., 2015. Impact of degrading permafrost on subsurface solute transport pathways and travel times. Water Resour. Res. 51 (9), 7680–7701.
Fujita, K., Ageta, Y., 2000. Effect of summer accumulation on glacier mass balance on the Tibetan Plateau revealed by mass-balance model. J. Glaciol. 46 (153), 244–252.
Gebremichael, M., Rigon, R., Bertoldi, G., Over, T.M., 2009. On the scaling characteristics of observed and simulated spatial soil moisture fields. Nonlin. Processes Geophys. 16 (1), 141–150.
Guo, W., Liu, S., Xu, J., Wu, L., Shangguan, D., Yao, X., Wei, J., Bao, W., Yu, P., Liu, Q., 2015. The second Chinese glacier inventory: data, methods and results. J. Glaciol. 61 (226), 357–372.
Gupta, H.V., Kling, H., Yilmaz, K.K., Martinez, G.F., 2009. Decomposition of the mean squared error and NSE performance criteria: Implications for improving hydrological modelling. J. Hydrol. 377 (1), 80–91.
Hinzman, L.D., Kane, D.L., Benson, C.S., Everett, K.R., 1996. In: Landscape Function and Disturbance in Arctic Tundra. Springer, Berlin Heidelberg, Berlin, Heidelberg, pp. 131–154.
Hinzman, L., Viereck, L.A., Adams, P.C., Romanovsky, V., Yoshikawa, K., 2006. Climate and permafrost dynamics of the Alaskan boreal forest. Alaska's Changing Boreal Forest 39–61.
Hu, P., Cai, T., Sui, F., Duan, L., Man, X., Cui, X., 2021. Response of Runoff to Extreme Land Use Change in the Permafrost Region of Northeastern China. Forests 12 (8), 1021.
Hülsmann, L., Geyer, T., Schweitzer, C., Priess, J., Karthe, D., 2015. The effect of subarctic conditions on water resources: initial results and limitations of the SWAT model applied to the Kharaa River Basin in Northern Mongolia. Environ. Earth Sci. 73 (2), 581–592.
Immerzeel, W.W., van Beek, L.P.H., Bierkens, M.F.P., 2010. Climate Change Will Affect the Asian Water Towers. Science 328 (5984), 1382–1385.
Jiang, Y., Zhuang, Q., O'Donnell, J.A., 2012. Modeling thermal dynamics of active layer soils and near-surface permafrost using a fully coupled water and heat transport model. J. Geophys. Res.: Atmos. 117 (D11).
Jin, H.J., Chang, X.L., Wang, S.L., 2007. Evolution of permafrost on the Qinghai-Xizang (Tibet) Plateau since the end of the late Pleistocene. J. Geophys. Res. Earth Surf. 112 (F2).
Just, L., 2020. Snow distribution and melt of a seasonal snowpack, Central Otago, New Zealand, University of Otago.
Krogh, S.A., Pomeroy, J.W., Marsh, P., 2017. Diagnosis of the hydrology of a small Arctic basin at the tundra-taiga transition using a physically based hydrological model. J. Hydrol. 550, 685–703.
Kudryavtsev, V., Garagulya, L. and Melamed, V., 1977. Fundamentals of Frost Forecasting in Geological Engineering Investigations (Osnovy Merzlotnogo Prognoza pri Inzhenerno-Geologicheskikh Issledovaniyakh), Cold Regions Research and Engineering Lab Hanover NH.
Kudryavtsev, V., Garagula, L., Kondratyeva, V., 1974. Foundation of Geocryology. Moscow State University Press, Moscow.

Magnusson, J., Wever, N., Essery, R., Helbig, N., Winstral, A., Jonas, T., 2015. Evaluating snow models with varying process representations for hydrological applications. Water Resour. Res. 51 (4), 2707–2723.
Mao, T., Wang, G., Zhang, T., 2016. Impacts of Climatic Change on Hydrological Regime in the Three-River Headwaters Region, China, 1960–2009. Water Resour. Manage. 30 (1), 115–131.
Marhaento, H., Booij, M., Hoekstra, A., 2018. Hydrological response to future land-use change and climate change in a tropical catchment. Hydrol. Sci. J. 63, 1368–1385.
McNamara, J.P., Kane, D.L., Hinzman, L.D., 1998. An analysis of streamflow hydrology in the Kuparuk River Basin, Arctic Alaska: a nested watershed approach. J. Hydrol. 206 (1), 39–57.
Melaku, N.D., Wang, J., Meshesha, T.W., 2020. Improving hydrologic model to predict the effect of snowpack and soil temperature on carbon dioxide emission in the cold region peatlands. J. Hydrol. 587, 124939.
Moriasi, N.D., G. Arnold, J., W. Van Liew, M., L. Bingner, R., D. Harmel, R. and L. Veith, T. 2007. Model Evaluation Guidelines for Systematic Quantification of Accuracy in Watershed Simulations. Trans. ASABE 50(3), 885-900.
Nasab, M.T., Chu, X., 2020. Do sub-daily temperature fluctuations around the freezing temperature alter macro-scale snowmelt simulations? J. Hydrol. 125683.
Nash, J.E., Sutcliffe, J.V., 1970. River flow forecasting through conceptual models part I — A discussion of principles. J. Hydrol. 10 (3), 282–290.
Nicolle, P., Pushpalatha, R., Perrin, C., François, D., Thiéry, D., Mathevet, T., Le Lay, M., Besson, F., Soubeyroux, J.M., Viel, C., Regimbeau, F., Andréassian, V., Maugis, P., Augeard, B., Morice, E., 2014. Benchmarking hydrological models for low-flow simulation and forecasting on French catchments. Hydrol. Earth Syst. Sci. 18 (8), 2829–2857.
Nie, N., Zhang, W., Liu, M., Chen, H., Zhao, D., 2020. Separating the impacts of climate variability, land-use change and large reservoir operations on streamflow in the Yangtze River basin, China, using a hydrological modeling approach. Int. J. Digital Earth 1–19.
Osuch, M., Wawrzyniak, T., Nawrot, A., 2019. Diagnosis of the hydrology of a small Arctic permafrost catchment using HBV conceptual rainfall-runoff model. Hydrol. Res. 50 (2), 459–478.
Pomeroy, J., Fang, X., Ellis, C., 2012. Sensitivity of snowmelt hydrology in Marmot Creek, Alberta, to forest cover disturbance. Hydrol. Process. 26 (12), 1891–1904.
Pomeroy, J.W., Gray, D.M., Brown, T., Hedstrom, N.R., Quinton, W.L., Granger, R.J., Carey, S.K., 2007. The cold regions hydrological model: a platform for basing process representation and model structure on physical evidence. Hydrol. Process. 21 (19), 2650–2667.
Qin, Y., Yang, D., Gao, B., Wang, T., Chen, J., Chen, Y., Wang, Y., Zheng, G., 2017. Impacts of climate warming on the frozen ground and eco-hydrology in the Yellow River source region, China. Sci. Total Environ. 605–606, 830–841.
Rigon, R., Bertoldi, G., Over, T.M., 2006. GEOtop: A Distributed Hydrological Model with Coupled Water and Energy Budgets. J. Hydrometeorol. 7 (3), 371–388.
Romanovsky, V.E., Smith, S.L., Christiansen, H.H., 2010. Permafrost thermal state in the polar Northern Hemisphere during the international polar year 2007–2009: a synthesis. Permafrost Periglac. Process. 21 (2), 106–116.
Schramm, I., Boike, J., Bolton, W.R., Hinzman, L.D., 2007. Application of TopoFlow, a spatially distributed hydrological model, to the Imnavait Creek watershed, Alaska. J. Geophys. Res.: Biogeosci. 112 (G4).
Schulla, J. and Jasper, K. 2007. Model description wasim-eth. Institute for Atmospheric and Climate Science, Swiss Federal Institute of Technology, Zürich.
Schulla, J., 1997. Hydrologische Modellierung von Flussgebieten zur Abschätzung der Folgen von Klimaänderungen, ETH Zurich.
Serreze, M.C., Barry, R.G., 2011. Processes and impacts of Arctic amplification: A research synthesis. Global Planet. Change 77 (1), 85–96.
Smith, M., Riseborough, D., 1996. Permafrost monitoring and detection of climate change. Permafrost Periglac. Process. 7 (4), 301–309.
Song, C., Wang, G., Mao, T., Dai, J., Yang, D., 2020. Linkage between permafrost distribution and river runoff changes across the Arctic and the Tibetan Plateau. Sci. China Earth Sci. 63 (2), 292–302.
Walvoord, M.A. and Kurylyk, B.L. 2016. Hydrologic Impacts of Thawing Permafrost—A Review. Vadose Zone J. 15(6), vzj2016.2001.0010.
Walvoord, M.A., Voss, C.I., Wellman, T.P., 2012. Influence of permafrost distribution on groundwater flow in the context of climate-driven permafrost thaw: Example from Yukon Flats Basin, Alaska, United States. Water Resour. Res. 48 (7).
Wang, G., Cheng, G., 2001. Characteristics of grassland and ecological changes of vegetations in the source regions of Yangtze and Yellow Rivers. J. Desert Res. 21 (2), 101–107.
Wang, G., Li, Y., Wang, Y., Shen, Y., 2007. Impacts of alpine ecosystem and climate changes on surface runoff in the headwaters of the Yangtze River. J. Glaciol. Geocryol. 29 (2), 159–168.
Wawrzyniak, T., Osuch, M., Nawrot, A., Napiorkowski, J.J., 2017. Run-off modelling in an Arctic unglaciated catchment (Fuglebekken, Spitsbergen). Ann. Glaciol. 58 (75pt1), 36–46.
Williams, J.R., 1970. Ground water in the permafrost regions of Alaska. US Government Printing Office.
Woo, M.-K., 2012a. Permafrost Hydrology. Springer, Berlin Heidelberg, Berlin, Heidelberg, pp. 163–227.
Woo, M.-K., 2012b. Permafrost Hydrology. Springer, Berlin Heidelberg, Berlin, Heidelberg, pp. 1–34.
Woo, M.-K., Kane, D.L., Carey, S.K., Yang, D., 2008. Progress in permafrost hydrology in the new millennium. Permafrost Periglac. Process. 19 (2), 237–254.
Woo, M.-K., Winter, T.C., 1993. The role of permafrost and seasonal frost in the hydrology of northern wetlands in North America. J. Hydrol. 141 (1–4), 5–31.
Woo, M.k., Marsh, P. and Pomeroy, J.W. 2000. Snow, frozen soils and permafrost hydrology in Canada, 1995–1998. Hydrological Processes 14(9), 1591-1611.
Wu, Q., Zhang, T., Liu, Y., 2010. Permafrost temperatures and thickness on the Qinghai-Tibet Plateau. Global Planet. Change 72 (1), 32–38.
Yang, J., Ding, Y.J., Chen, R.S., Yp, S., 2002. Permafrost change and its effect on eco-environment in the source regions of the Yangtze and Yellow Rivers. J. Mountain Sci. 22 (1), 33–39.
Zhang, Y., Wang, X., Fraser, R., Olthof, I., Chen, W., McLennan, D., Ponomarenko, S., Wu, W., 2013. Modelling and mapping climate change impacts on permafrost at high spatial resolution for an Arctic region with complex terrain. The Cryosphere 7 (4), 1121–1137.
Zhang, Z., Wu, Q., 2012. Predicting changes of active layer thickness on the Qinghai-Tibet Plateau as climate warming. J. Glaciol. Geocryol. 34 (3), 505–511.
Zhao, D., Wu, S., 2019. Projected Changes in Permafrost Active Layer Thickness Over the Qinghai-Tibet Plateau Under Climate Change. Water Resour. Res. 55 (9), 7860–7875.
Zhou, J., Kinzelbach, W., Cheng, G., Zhang, W., He, X., Ye, B., 2013. Monitoring and modeling the influence of snow pack and organic soil on a permafrost active layer, Qinghai-Tibetan Plateau of China. Cold Reg. Sci. Technol. 90–91, 38–52.